ORIGINAL ARTICLE

Contrast-enhanced CT-based radiomic analysis for determining the response to anti-programmed death-1 therapy in esophageal squamous cell carcinoma patients: A pilot study

Qinzhu Yang[1] | Haofan Huang[1,2] | Guizhi Zhang[3] | Nuoqing Weng[4] |
Zhenkai Ou[1] | Meili Sun[5] | Huixing Luo[4] | Xuhui Zhou[3] | Yi Gao[1,6,7] |
Xiaobin Wu[4]

[1]School of Biomedical Engineering, Shenzhen University Medical School, Shenzhen University, Shenzhen, China

[2]Department of Biomedical Engineering, Hong Kong Polytechnic University, Hong Kong SAR, China

[3]Department of Radiology, The Eighth Affiliated Hospital of Sun Yat-sen University, Shenzhen, China

[4]Department of Gastrointestinal Surgery, The Eighth Affiliated Hospital, Sun Yat-sen University, Shenzhen, China

[5]Department of Radiology, Sun Yat-sen University Cancer Center, State Key Laboratory of Oncology in South China, Collaborative Innovation Center for Cancer Medicine, Guangzhou, China

[6]Shenzhen Key Laboratory of Precision Medicine for Hematological Malignancies, Shenzhen, China

[7]Marshall Laboratory of Biomedical Engineering, Shenzhen, China

Correspondence
Xuhui Zhou, Yi Gao and Xiaobin Wu, Department of Radiology, The Eighth Affiliated Hospital of Sun Yat-sen University, Shenzhen, China, School of Biomedical Engineering, Shenzhen University Medical School, Shenzhen University, Shenzhen 518055, China, and Department of Gastrointestinal Surgery, The Eighth Affiliated Hospital, Sun Yat-sen University, Shenzhen, China.
Email: zhouxuh@mail.sysu.edu.cn;
gaoyi@szu.edu.cn; and
Email: wuxiaob2@mail.sysu.edu.cn

Abstract

Background: In view of the fact that radiomics features have been reported as predictors of immunotherapy to various cancers, this study aimed to develop a prediction model to determine the response to anti-programmed death-1 (anti-PD-1) therapy in esophageal squamous cell carcinoma (ESCC) patients from contrast-enhanced CT (CECT) radiomics features.

Methods: Radiomic analysis of images was performed retrospectively for image samples before and after anti-PD-1 treatment, and efficacy analysis was performed for the results of two different time node evaluations. A total of 68 image samples were included in this study. Quantitative radiomic features were extracted from the images, and the least absolute shrinkage and selection operator method was applied to select radiomic features. After obtaining selected features, three classification models were used to establish a radiomics model to predict the ESCC status and efficacy of therapy. A cross-validation strategy utilizing three folds was employed to train and test the model. Performance evaluation of the model was done using the area under the curve (AUC) of receiver operating characteristic, sensitivity, specificity, and precision metric.

Results: Wavelet and area of gray level change (log-sigma) were the most significant radiomic features for predicting therapy efficacy. Fifteen radiomic features from the whole tumor and peritumoral regions were selected and comprised of the fusion radiomics score. A radiomics classification was developed with AUC of 0.82 and 0.884 in the before and after-therapy cohorts, respectively.

Conclusions: The combined model incorporating radiomic features and clinical CECT predictors helps to predict the response to anti-PD-1therapy in patients with ESCC.

KEYWORDS
esophageal squamous cell carcinoma, machine learning, tomography, x-ray computed

INTRODUCTION

Esophageal carcinoma (EC) is a major cause of cancer-related death globally,[1] with ESCC being the predominant subtype in China.[2] Early detection of ESCC is challenging, leading to advanced diagnoses that restrict surgical options. Hence, alternative treatments like chemotherapy[3] and immunotherapy[4] are pivotal for managing this disease.

In recent years, programmed death 1/programmed death ligand 1 (PD-1/PD-L1) inhibitor therapy[5,6] has shown promise in treating ESCC,[7–9] but it is costly and may result in severe immune-related side effects. Hence, identifying patients who are likely to benefit from immunotherapy before treatment is critical.[10] However, the use of immunohistochemistry biomarkers[11,12] as predictive biomarkers are limited due to intratumoral heterogeneity and evolution over time.[13,14]

Alternately, some research focuses on using blood biomarkers to predict the response of ESCC patients to anti-PD-1 therapy.[15–17] While these biomarkers have been identified as prognostic indicators for ESCC risk stratification and therapy decision-making, they overlook critical information on tumors.[18]

Radiomics is a potentially valuable approach to extracting valuable data from computational medical images, providing a noninvasive option for assessing tumors and their immune microenvironment[19,20] as an alternative to biopsy. CT imaging is commonly utilized for cancer evaluation, particularly CECT for detecting primary tumors and lymph nodes in esophageal cancer patients.[21]

Our previous study[22] investigated using peripheral blood parameters to assess ESCC patient response to anti-PD-1 therapy combined with other treatments. While feasible, utilizing radiomic features from CECT images provides a more precise evaluation method, as they accurately depict tumor size and grayscale changes over time. Therefore, efficient acquisition, modeling, and analysis of these images of tumors are necessary.

Machine learning (ML) is a promising tool for extracting valuable information from clinical data, offering a solution for addressing the challenges in the prediction of PD-1/PD-L1 response and efficacy evaluation.[23] Similar to this idea of biomarker discovery in terms of radiomic features with the ML method, there have been some studies on different diseases.[10,24–26] However, few studies have evaluated the role of CECT-based radiomic features in ESCC patients treated with anti-PD-1.

To fill this gap, we conducted a pilot retrospective study of 40 ESCC patients treated with PD-1 inhibitors. In this study, our objective was to develop a reliable and practical radiomic index that can predict and evaluate the response to anti-PD-1 combination therapy in ESCC patients at different treatment stages.

METHODS

Patients and assessment

This study conducted a pilot retrospective analysis of 40 patients with ESCC who were treated with anti-PD-1 inhibitor therapy in our hospital between December 2018 and September 2020. This study was approved by the Institutional Review Board of our hospital. All patients provided written-informed consent for the collection and publication. The objective of the study was to investigate changes in tumor characteristics observed on computed tomography (CT) images before and after treatment. To ensure appropriate case selection, patients who underwent surgical resection before treatment evaluation were excluded from the analysis. According to RECIST (solid tumor response assessment criteria) version 1.1, radiological examinations were first performed to evaluate the effect of immunotherapy at 8–12 weeks. The last available data for further updates on patient responses was before April 2022, which is set as the second time record of the response. There are therefore two-time node records of the response to the treatment.
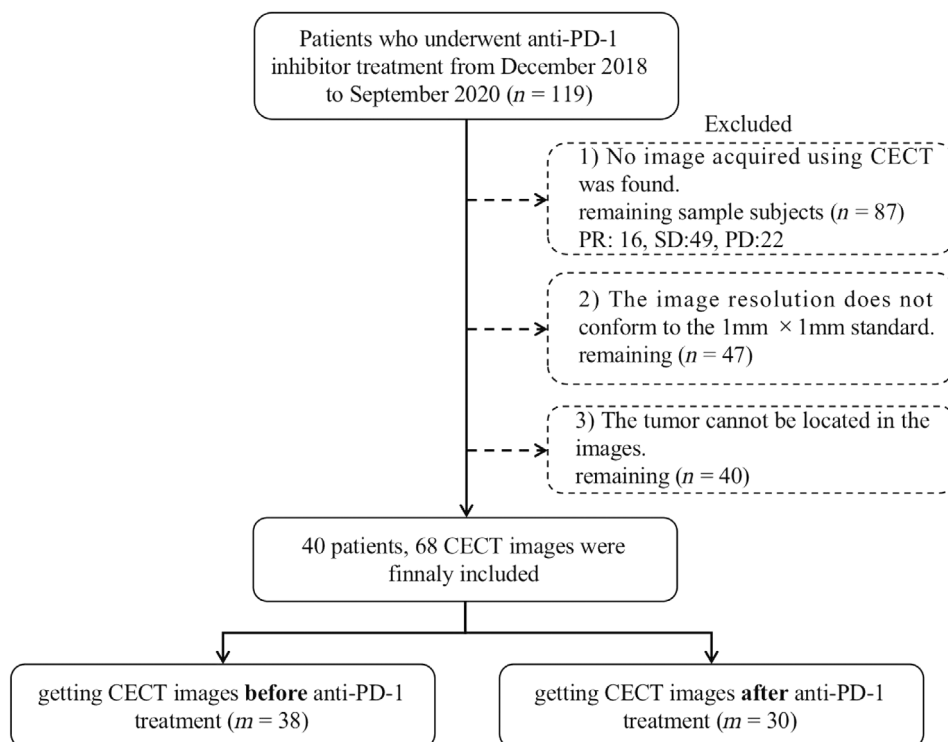
CECT image acquisition

All CT scans were performed using 64-slice multidetector CT scanners (Gold Discovery CT750 HD; GE Healthcare). The following scanning parameters were employed: 120 kVp; automatic in the range 50–360 mA; 64×0.625 mm detector collimation; 512×512 matrix size; the helical pitch of 0.984; and 1.25 mm slice thickness. Contrast-enhanced CT (CECT) images were obtained 75 s after the intravenous administration at a dose of 1.2 mL/kg and an injection rate of 2–2.5 mL/s. Before treatment initiation, patients underwent CECT scanning of the chest, abdomen, and neck for radiological assessment. Images with a resolution of about 1 mm³ were selected to ensure optimal image quality.

In the image preprocessing stage, we use the python library SimpleITK to process slices of the volumetric image and to output the corresponding volume. All images were adjusted according to the window location and window width set at 40 and 350. In a few cases, in order to facilitate a better display of the tumor area, small adjustments were made to the values of the window width and location.

Tumor segmentation and radiomic feature extraction

Following image acquisition, we performed tumor segmentation and radiomic feature extraction. Initially, two physicians, each possessing 3–5 years of experience, manually delineated the tumor on the CECT images using the 3D Slicer software (https://www.slicer.org). To account for the heterogeneity of the tumor, the delineated 3D tumor ROI

Patients who underwent anti-PD-1 inhibitor treatment from December 2018 to September 2020 ($n = 119$)

Excluded

1) No image acquired using CECT was found.
remaining sample subjects ($n = 87$)
PR: 16, SD:49, PD:22

2) The image resolution does not conform to the 1mm × 1mm standard.
remaining ($n = 47$)

3) The tumor cannot be located in the images.
remaining ($n = 40$)

40 patients, 68 CECT images were finnaly included

getting CECT images **before** anti-PD-1 treatment ($m = 38$)

getting CECT images **after** anti-PD-1 treatment ($m = 30$)

FIGURE 1 Flow diagram of the participants included in this study. The letter n represents the number of patients, and the letter m represents the number of contrast-enhanced computed tomography (CECT) images.
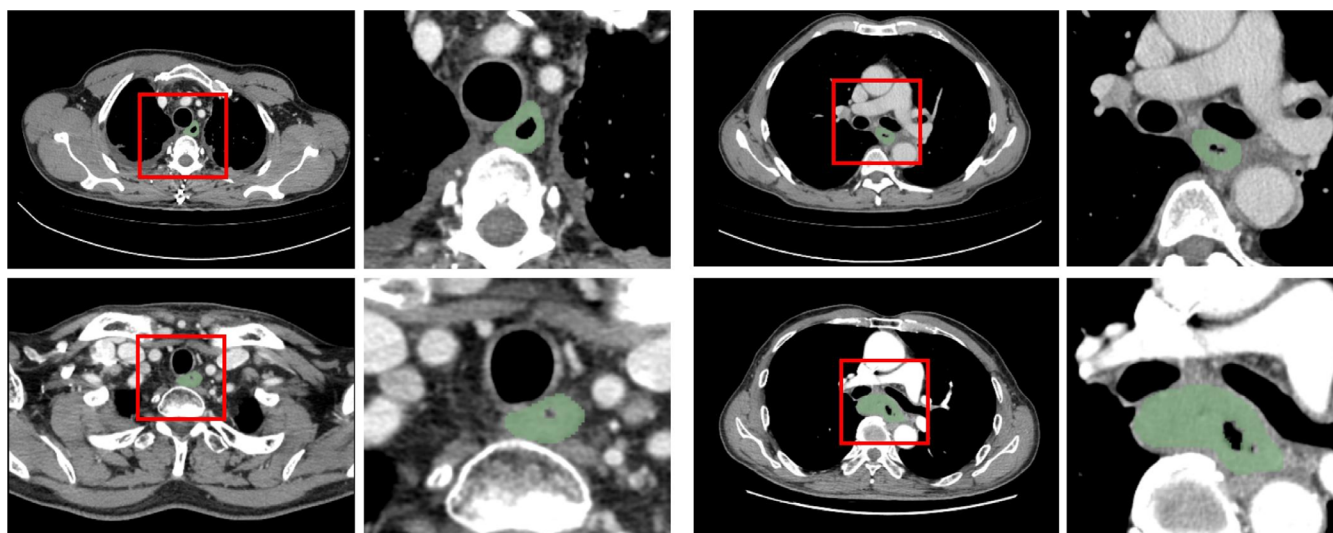
FIGURE 2 Annotated tumor maps of four patients included in the study. The top row illustrates images obtained after the treatment of two patients, while the bottom row exhibits images obtained before the treatment of the other two patients. The delineated green annotation represents the specific region of the tumor. The second and fourth columns present magnified views of the areas outlined by the red frames in the first and third columns, respectively.

encompassed the entire lesion, including the internal necrotic area. In case of disagreement, a higher-level physician was consulted to confirm the delineation, thereby reducing interindividual variation. Using the aforementioned approach (explained in detail in Figure 1), we filtered the data and obtained annotations for a total of 68 image samples. For visualization, we also show the segmentation results corresponding to the four samples in Figure 2.

After obtaining the segmented tumor annotations, the radiomic features were computed. We used the open-source software PyRadiomics[27] to extract radiographic features. A total of 1218 candidate radiomic features were extracted from each CECT sample. These included 22 classes of gray-level co-occurrence matrices (GLCM), 16 classes of gray-level run-length matrices (GLRLM), 14 classes of gray-level dependency matrices (GLDM), 16 classes of gray-

level size zone matrices (GLSZM), 18 classes of first order statistics features and one class of shape-based feature.

Grouping two dynamic time nodes of image acquisition and two treatment effect classification

After filtering the dataset, the remaining 68 samples were divided into two groups based on the time nodes, as they had images before and after the anti-PD-1 treatment. Among the samples, 38 image samples were collected before the treatment, and the remaining 30 samples were collected after the treatment. The two images before and after the anti-PD-1 treatment time nodes were then used to create a dynamic image node as illustrated in Figure 3.

In addition to the aforementioned grouping of dynamic image nodes, we also included dynamic efficacy evaluation groupings based on the first 8–12 weeks of efficacy evaluation results and the latest follow-up diagnosis and treatment results. This dynamic change in efficacy can be utilized as an important criterion for screening the features.

Clinical response was defined as either partial remission (PR) or stable disease (SD), while nonclinical response was

FIGURE 3 Illustration of two time node records of treatment efficacy and two time node records of image acquisition. Character R represents the clinical response and N represents the nonclinical response. Group A and group B represent the different groups.
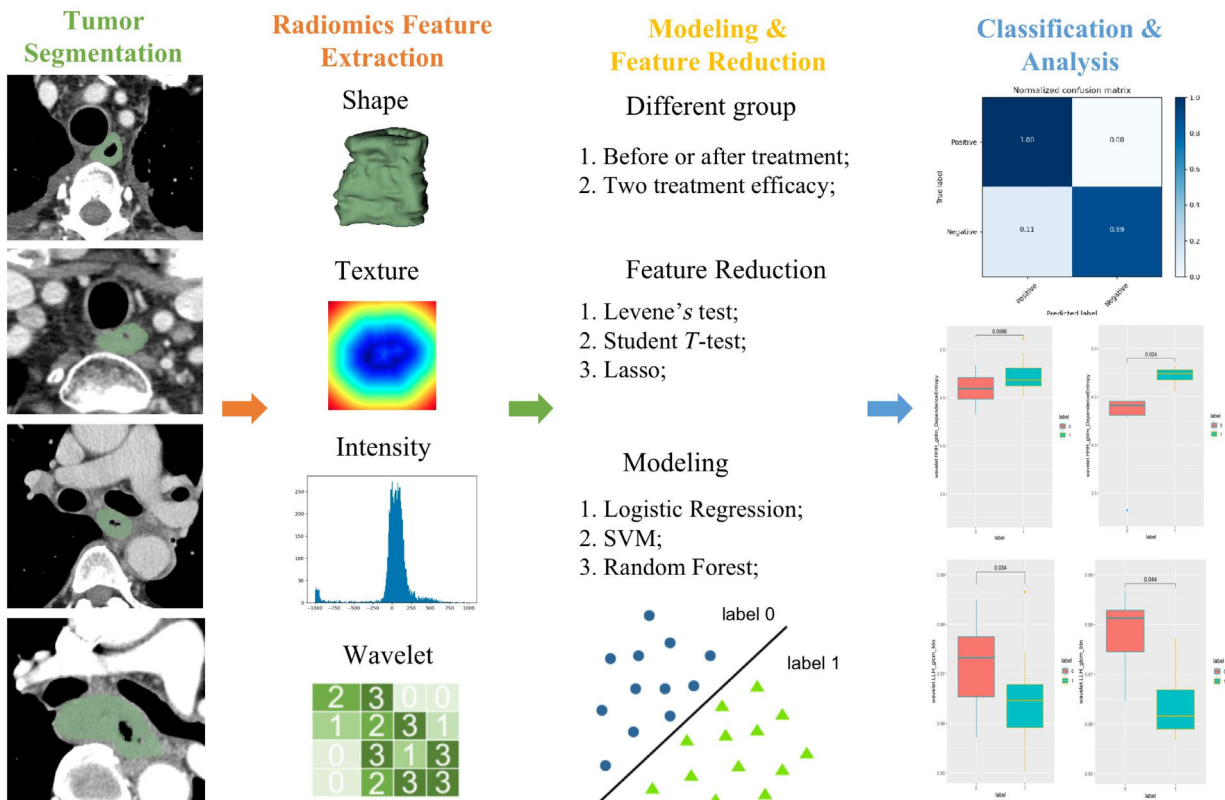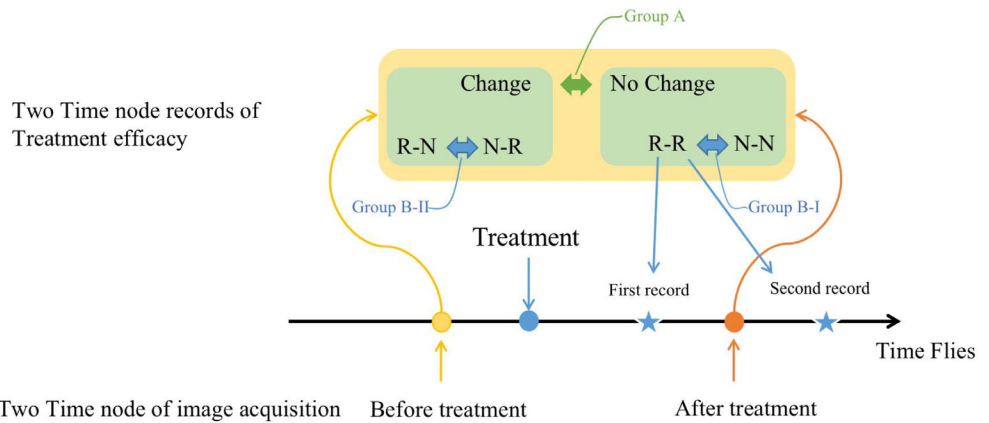
FIGURE 4 Radiomics prediction workflow for the response to anti-PD-1 therapy in ESCC.

defined as progressive disease (PD). The groups were initially divided based on images before and after treatment. In group A, samples were labeled as negative (label 0) if the results of the two treatment efficacy queries were consistent, whereas samples that displayed a change were labeled as positive (label 1). In group B, the invariant samples from group A were further subdivided. For instance, samples with the same treatment response (e.g., from clinical response to clinical response) were labeled as negative (label 0), while samples with changed treatment response were labeled as positive (label 1). The above-described process was carried out to ensure consistency and accuracy in sample categorization.

Modeling and statistical analysis

As the number of features obtained was more than 1200, we needed to select a subset of features for subsequent classification tasks. This was done through three sequential steps. First, Levene's test method was applied to evaluate the equality of variances for variables in different groups, and the student's t-test method was used to select the features with significant differences (p-value less than 0.05). Second, the least absolute shrinkage and selection operator (LASSO) method was employed to identify the most useful features using the training set. Finally, machine learning classification models, such as logistic regression (LR), support vector machine (SVM), or random forest (RF), were used to classify. Performance evaluation of the radiomics model was done using the area under the curve (AUC) of receiver operating characteristic, sensitivity, specificity, and precision metric. This enables convenient analysis of the effectiveness of anti-PD-1 treatment in the different groups mentioned above. The prediction and analysis workflow is presented in Figure 4.

In the classification process, the small sample size led to an imbalanced proportion of negative and positive data, which increased the possibility of false negative prediction results. To address this issue, two steps were taken. First, the data were normalized, and random upsampling was applied to balance the proportion of positive and negative samples. The upsampling processes was executed in Imblearn toolbox[28] using Python programming language. For reproducibility, the random seed was set to 1234. Second, a three-fold cross-validation method was used to train and validate the model while maintaining the negative–positive ratio. The purpose of this approach was to ensure that the model was robust and accurate, despite the imbalanced nature of the data.

Due to the limited number of sample subjects, it was not possible to construct a classification model for both two group B. To address this limitation, feature reduction and selection methods were utilized to identify salient features present in both group A and group B. This approach enabled the identification of potential information on changes in the sample data. The feature distribution was

analyzed using box plots to facilitate viewing and statistical analysis, which was performed using the R software. The objective of this approach was to optimize the analysis of the data and to mitigate the limitations associated with the small sample size.

RESULTS

The baseline characteristics of participants in the group before or after the treatment are presented in Table 1. A total of 68 sampled images from 40 participants were enrolled and allocated to these two groups. There were no

TABLE 1 The baseline characteristics of the groups before or after treatment.

Variable	Group before treatment ($m = 38$)	Group after treatment ($m = 30$)	p-value
Age (years)	62 ± 8	62 ± 7	0.956[a]
Gender			0.869[b]
Male	31 (81.58%)	24 (80.00%)	
Female	7 (18.42%)	6 (20.00%)	
Smoking			0.878[b]
Yes	26 (68.42%)	20 (66.67%)	
No	12 (31.58%)	10 (33.33%)	
Alcohol drinking			0.813[b]
Yes	23 (60.53%)	19 (63.33%)	
No	15 (39.47%)	11 (36.67%)	
Family history of cancer			0.924[b]
Yes	11 (28.95%)	9 (30.00%)	
No	27 (71.05%)	21 (70.00%)	
Response of patients (first record)			0.572[b]
PR/SD	31 (81.58%)	26 (86.67%)	
PD	7 (18.42%)	4 (13.33%)	
Response of patients (second record)			0.602[b]
PR/SD	27 (71.05%)	23 (76.67%)	
PD	11 (28.95%)	7 (23.33%)	
Tumor location			0.839[b]
Up	14 (36.84%)	13 (43.33%)	
Medium	15 (39.48%)	10 (33.33%)	
Low	9 (23.68%)	7 (23.34%)	
Maximum 3D diameter (cm)	7.58 ± 3.4	5.71 ± 2.27	0.012[a,*]
Mesh volume (cm^3)	30.22 ± 31.3	13.95 ± 13.65	0.005[a,**]

Note: Unless otherwise indicated, data in parentheses are percentages; m, number of samples participants.
Abbreviations: PD, progressive disease; PR, partial remission; SD, stable disease.
[a]p-value was calculated with student's t-test.
[b]p-value was calculated with Pearson's chi-squared test without applying Yates' correction.
*$p < 0.05$; **$p < 0.01$.

T A B L E 2 Group information of this study.

Group name	Label	Group name	Label
Group A Before (After) treatment	Label 0: No changes in response (clinical response to clinical response, nonclinical response to nonclinical response)	Group B–I	Label 0: Clinical response to clinical response
			Label 1: Nonclinical response to nonclinical response
	Label 1: Changes in response (nonclinical response to clinical response, clinical response to nonclinical response)	Group B–II	Label 0: Nonclinical response to clinical response
			Label 1: Clinical response to nonclinical response

Note: Group A: The group information of the response of patients before or after treatment, the response of patients that did not change between 6 weeks and subsequent follow-up observations are marked with label 0, and those that had changed are marked with label 1. Groups B–I: Samples are from label 0 in group A. Groups B–II: Samples are from label 1 in group A.

T A B L E 3 The classification results (mean and standard deviation) of predicting changes in treatment efficacy are based on the screening characteristics of group A before and after treatment.

	Before/after treatment	AUC (95% CI)	Accuracy	Sensitivity	Specificity	Precision
SVM	Before	0.672 ± 0.153 [0.197–0.913]	0.665 ± 0.159	0.478 ± 0.282	0.867 ± 0.188	0.852 ± 0.209
	After	0.847 ± 0.119 [0.819–1.0]	0.843 ± 0.120	0.889 ± 0.157	0.806 ± 0.141	0.826 ± 0.123
RF	Before	0.820 ± 0.061 [0.671–1.0]	0.822 ± 0.064	0.926 ± 0.104	0.715 ± 0.046	0.761 ± 0.054
	After	0.884 ± 0.080 [0.687–1.0]	0.881 ± 0.082	0.889 ± 0.157	0.88 ± 0.006	0.878 ± 0.014
LR	Before	0.770 ± 0.149 [0.5–0.922]	0.768 ± 0.150	0.819 ± 0.107	0.722 ± 0.207	0.758 ± 0.186
	After	0.861 ± 0.019 [0.833–1.0]	0.86 ± 0.026	0.917 ± 0.117	0.806 ± 0.141	0.848 ± 0.113

Abbreviations: CI, confidence interval; LR, logistic regression; RF, random forest; SVM, support vector machine.

statistically significant differences in age, gender, smoking, alcohol drinking, family history of cancer, and tumor location among patients before and after treatment ($p > 0.05$). The study utilized the group setting as outlined in Table 2 according to the clinical response of treatment. The LASSO and t-test methods were applied to group and filter 1218 features extracted by PyRadiomics. This approach resulted in the identification of 15 significant features that were selected for subsequent analysis. These features were used to classify changes in treatment efficacy, specifically whether there was a change from response to nonresponse or from nonclinical response to clinical response. The selected features were considered to be of high importance and enabled a focused and targeted analysis of the data. This approach was designed to optimize the analysis process and increase the accuracy of the classification model. Logistic regression, SVM, and RF methods were separately used to establish the radiomics model. The model established by the RF method yielded the best performance in most metrics in three-fold cross validation, and the results are shown in Table 3.

The mean AUC values achieved in the first two rows of the table were 0.82 and 0.884, respectively. These results suggest that it is possible to use CECT images obtained before and after the treatment for the prospective assessment of changes in treatment efficacy, specifically whether there is a change from response to non-response or vice versa. However, the other two classifiers had much higher AUC in the group after treatment than in the group before treatment, indicating that the results were influenced by

T A B L E 4 Features extracted from images obtained before/after treatment.

Before/after treatment	Feature names
Before	Wavelet-LHH_gldm_DependenceNonUniformityNormalized
	Wavelet-LHH_glcm_ClusterProminence
	Log-sigma-5-0-mm-3D_glrlm_LongRunLowGrayLevelEmphasis
	Wavelet-LHH_gldm_DependenceVariance
	Wavelet-LHH_gldm_DependenceEntropy
After	Log-sigma-4-0-mm-3D_firstorder_Maximum
	Wavelet-HHL_firstorder_Median
	Wavelet-LLL_glcm_Idmn
	Wavelet-LHL_glcm_Correlation
	Wavelet-HHL_gldm_DependenceNonUniformityNormalized
	Wavelet-HHH_glcm_Idmn
	Wavelet-HHH_glcm_Idn
	Wavelet-HHH_glrlm_LongRunLowGrayLevelEmphasis
	Wavelet-HHH_glszm_SmallAreaLowGrayLevelEmphasis
	Wavelet-HHH_glrlm_ShortRunLowGrayLevelEmphasis

Note: They are repeated in both group A and group B. LHH, HHL, LLL, LHL, HHH are frequency channels; L and H are low- and high-pass filters, respectively.

category imbalance and model overfitting. Despite these limitations, the study demonstrated the potential of using machine learning techniques to analyze medical imaging data and make clinically relevant predictions.

The 15 features identified in this study were found to have statistically significant differences between the categorical variables in both groups A and B. These features can provide valuable information on changes in treatment efficacy, and box plots of their feature distributions were created under different groups. Table 4 summarizes these features, with five significant features extracted from CECT images acquired before treatment and 10 features with significant differences from images after treatment.

To investigate the relationship between changes in treatment efficacy and radiomic features before and after treatment, as well as during the first and second time treatment efficacy queries, we analyzed the distribution of radiomic features in different groups according to the grouping strategy outlined in Table 2. The results which are presented in

Figure 5 and Figure 6 provide insight into the changes in these features over time and how they relate to changes in treatment efficacy.

In Figure 5, we have presented the radiomic values of three distinct groups, which exhibit a consistent trend in both group A and groups B–I when labeled as either 0 or 1. Notably, lower values of these radiomic features may serve as indicators for better response to anti-PD-1 treatment. The p-value, representing the statistical significance of the t-test conducted on the target grouping, is less than 0.05 in all cases, thus indicating a significant difference.

To assess changes in treatment efficacy and image features obtained before and after treatment, we conducted a comparative analysis of box plots for two groups: from clinical response to clinical response and from clinical response
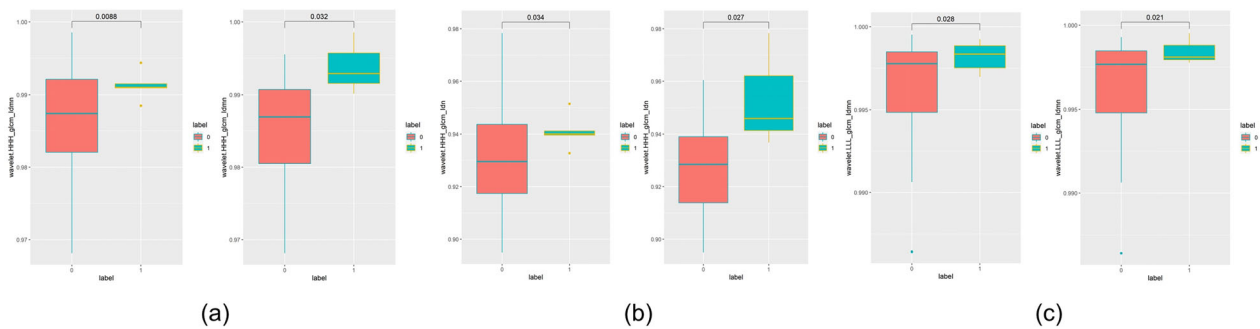
FIGURE 5 Box plots of wavelet radiomic features value three distinct groups within the after-treatment cohort. The left columns in subfigure (a)–(c) represent the values obtained from group A. The remaining right columns of each subfigure (a)–(c) display the values obtained from group B-I.
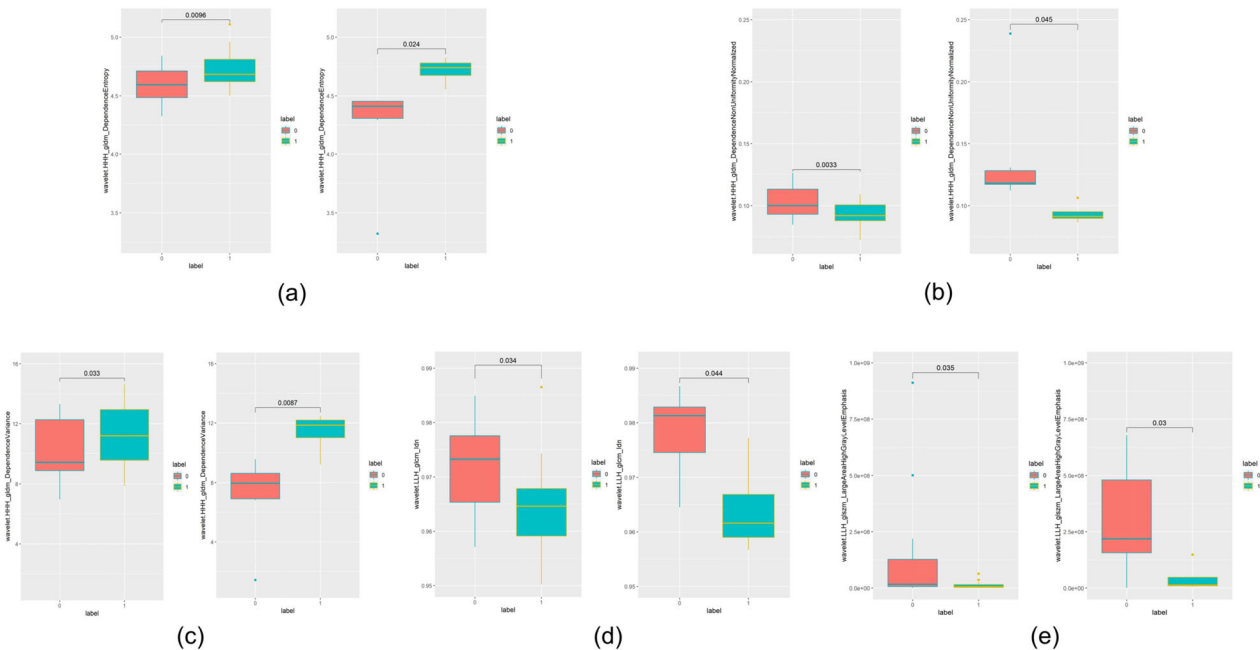
FIGURE 6 Comparison box plots of significant image features before and after treatment, focusing on efficacy changes across five groups. Subfigures (a)–(e) illustrate two groupings, one on the left for changes from clinical response to clinical response and the other on the right for changes from clinical response to nonclinical response. The labels used in this analysis were labeled 0 to denote features from images obtained before treatment images and labeled 1 to denote features from images obtained after treatment.

to nonclinical response. Figure 6 depicts these box plots, with label 0 indicating features in images obtained before treatment and label 1 representing features obtained after treatment. Our findings revealed that, across all subfigures in Figure 6, the difference between the box plots on the right was consistently greater than group on the left. This suggests that a larger difference in feature value range before and after treatment is more likely to correspond with a change in treatment efficacy from clinical to nonclinical response. Moreover, these changes in the tumor are wavelet feature information, particularly in features that experienced significant range variation. These observations suggest a decrease in treatment efficacy and indicate the emergence of progressive disease.

DISCUSSION AND CONCLUSION

This pilot study constructed a prediction model for the efficacy of anti-PD-1 treatment in patients with ESCC, utilizing 15 quantitative CECT radiomic features to evaluate treatment efficacy. These 15 radiomic features, including wavelet transformed features, first-order statistics features, and gray-level emphasis features, were identified and utilized to construct a radiomic signature model. Notably, these features offer a comprehensive approach for mining tumor heterogeneity information from images over time, thereby serving as a valuable tool for characterizing the spatial and temporal variations of tumor features. The classification results indicate that our proposed method exhibits good performance, with an AUC greater than 0.82, as evidenced by cross-validation on different datasets. These findings suggest that the developed radiomics model holds significant potential as a predictive tool for anti-PD-1 therapy response in ESCC patients, thus providing valuable insights for improving personalized cancer treatment.

Despite previous studies that have attempted to use biomarkers for predicting the efficacy of anti-PD-1 therapy, there has been a lack of research that directly utilizes tumor image information to provide more direct and observable feedback.[15–17] CECT-based information mining has demonstrated its utility in anti-PD-1/PD-L1 therapeutic efficacy in other diseases.[25,26] In this context, a CECT-based examination is a valuable tool as it offers a macroscopic and direct way to evaluate tumor characteristics in patients with esophageal cancer. Consequently, CECT examination can be utilized to identify tumor changes, perform preoperative evaluation, and predict treatment prognosis, thereby serving as a promising approach for improving patient outcomes.

The present study had some limitations that should be acknowledged. First, due to the limited availability of patient samples possessing both treatment record information and image information, the number of patients included in the study was relatively low. Future research involving a larger patient cohort would provide more robust evidence and increase the significance of the study. Second, the retrospective nature of the study meant that only CECT images were utilized. Future studies can expand the scope of imaging modalities to include other techniques such as MR images, which may enhance the clinical applicability of the findings. Lastly, the tumor segmentation method employed in the study was manual, which may have introduced potential biases. Future studies could explore the use of an automatic and repeatable segmentation method to improve the integration and full automation of the radiomic analysis.

The proposed radiomics model in this study, based on CECT imaging, demonstrates strong performance in predicting the efficacy of anti-PD-1 therapy in patients with ESCC. This model may have valuable implications for clinicians in screening ESCC patients who are likely to benefit from anti-PD-1 immunotherapy, thereby facilitating the provision of personalized treatment options. These findings may hold significant implications for the development of more effective and targeted cancer treatment strategies.

AUTHOR CONTRIBUTIONS
Qinzhu Yang: Methodology; writing–original draft/review and editing. **Haofan Huang:** Methodology; investigation. **Nuoqing Weng:** Resources; investigation; writing–review and editing. **Zhenkai Ou:** Methodology; software. **Guizhi Zhang:** Data curation. **Meili Sun:** Resources; writing–original draft. **Huixing Luo:** Resources; writing–original draft. **Xuhui Zhou:** Conceptualization; data curation; supervision. **Yi Gao:** Conceptualization; methodology, project administration; funding acquisition. **Xiaobin Wu:** Conceptualization; project administration; funding acquisition.

CONFLICT OF INTEREST STATEMENT
The authors declare that they have no conflicts of interest.

DATA AVAILABILITY STATEMENT
The datasets used and/or analyzed during the current study are available from the corresponding author on reasonable request.

ORCID

Yi Gao ⬤ https://orcid.org/0000-0003-0094-8136

REFERENCES

1. Siegel RL, Miller KD, Jemal A. Cancer statistics, 2019. CA Cancer J Clin. 2019;69(1):7–34. https://doi.org/10.3322/caac.21551
2. Liang H, Fan J-H, Qiao Y-L. Epidemiology, etiology, and prevention of esophageal squamous cell carcinoma in China. Cancer Biol Med. 2017;14(1):33–41. https://doi.org/10.20892/j.issn.2095-3941.2016.0093
3. Le Bras GF, Farooq MH, Falk GW, Andl CD. Esophageal cancer: the latest on chemoprevention and state of the art therapies. Pharmacol Res. 2016;113:236–44. https://doi.org/10.1016/j.phrs.2016.08.021
4. Kelly RJ. The emerging role of immunotherapy for esophageal cancer. Curr Opin Gastroenterol. 2019;35(4):337–43. https://doi.org/10.1097/MOG.0000000000000542
5. Lee NY, Ferris RL, Psyrri A, Haddad RI, Tahara M, Bourhis J, et al. Avelumab plus standard-of-care chemoradiotherapy versus chemoradiotherapy alone in patients with locally advanced squamous cell carcinoma of the head and neck: a randomised, double-blind, placebo-controlled, multicentre, phase 3 trial. Lancet Oncol. 2021; 22(4):450–62. https://doi.org/10.1016/S1470-2045(20)30737-3
6. Choueiri TK, Powles T, Burotto M, Escudier B, Bourlon MT, Zurawski B, et al. Nivolumab plus cabozantinib versus sunitinib for advanced renal-cell carcinoma. N Engl J Med. 2021;384(9):829–41. https://doi.org/10.1056/NEJMoa2026982
7. Petrillo A, Smyth EC. Immunotherapy for squamous esophageal cancer: a review. Journal of Personalized Medicine. 2022;12(6):862. https://doi.org/10.3390/jpm12060862
8. Chen K, Wang X, Yang L, Chen Z. The anti-PD-1/PD-L1 immunotherapy for gastric esophageal cancer: a systematic review and meta-analysis and literature review. Cancer Control. 2021;28: 1073274821997430. https://doi.org/10.1177/1073274821997430
9. Zhao Q, Yu J, Meng X. A good start of immunotherapy in esophageal cancer. Cancer Med. 2019;8(10):4519–26. https://doi.org/10.1002/cam4.2336
10. Wu M, Zhang Y, Zhang J, Zhang Y, Wang Y, Chen F, et al. A combined-radiomics approach of CT images to predict response to anti-PD-1 immunotherapy in NSCLC: a retrospective multicenter study. Front Oncol. 2022;11:688679. https://doi.org/10.3389/fonc.2021.688679
11. Nishino M, Hatabu H, Hodi FS. Imaging of cancer immunotherapy: current approaches and future directions. Radiology. 2019;290(1):9–22. https://doi.org/10.1148/radiol.2018181349
12. Wu M, Zhang Y, Zhang Y, Liu Y, Wu M, Ye Z. Imaging-based biomarkers for predicting and evaluating cancer immunotherapy response. Radiology: imaging. Cancer. 2019;1(2):e190031. https://doi.org/10.1148/rycan.2019190031
13. Jin Y, Shen X, Pan Y, Zheng Q, Chen H, Hu H, et al. Correlation between PD-L1 expression and clinicopathological characteristics of non-small cell lung cancer: a real-world study of a large Chinese cohort. J Thorac Dis. 2019;11(11):4591–601. https://doi.org/10.21037/jtd.2019.10.80
14. Heeke S, Hofman P. Tumor mutational burden assessment as a predictive biomarker for immunotherapy in lung cancer patients: getting ready for prime-time or not? Translational Lung Cancer Research. 2018;7(6):631–8. https://doi.org/10.21037/tlcr.2018.08.04
15. Zhang X, Gari A, Li M, Chen J, Qu C, Zhang L, et al. Combining serum inflammation indexes at baseline and post treatment could predict pathological efficacy to anti-PD-1 combined with neoadjuvant chemotherapy in esophageal squamous cell carcinoma. J Transl Med. 2022;20(1):1–11. https://doi.org/10.1186/s12967-022-03252-7
16. Jeyakumar G, Kim S, Bumma N, Landry C, Silski C, Suisham S, et al. Neutrophil lymphocyte ratio and duration of prior anti-angiogenic therapy as biomarkers in metastatic RCC receiving immune checkpoint inhibitor therapy. J Immunother Cancer. 2017;5(1):1–8. https://doi.org/10.1186/s40425-017-0287-5
17. Akutsu Y, Murakami K, Kano M, Toyozumi T, Matsumoto Y, Takahashi M, et al. The concentration of programmed cell death-ligand 1 in the peripheral blood is a useful biomarker for esophageal squamous cell carcinoma. Esophagus. 2018;15:103–8. https://doi.org/10.1007/s10388-018-0604-1
18. Matsumoto S, Wakatsuki K, Nakade H, Kunishige T, Miyao S, Tsujimoto A, et al. Impact of CT-assessed changes in tumor size after neoadjuvant chemotherapy on pathological response and survival of patients with esophageal squamous cell carcinoma. Langenbecks Arch Surg. 2022;407(3):965–74. https://doi.org/10.1007/s00423-022-02430-x
19. Gillies RJ, Kinahan PE, Hricak H. Radiomics: images are more than pictures, they are data. Radiology. 2016;278(2):563–77. https://doi.org/10.1148/radiol.2015151169
20. Limkin EJ, Sun R, Dercle L, Zacharaki EI, Robert C, Reuzé S, et al. Promises and challenges for the implementation of computational medical imaging (radiomics) in oncology. Ann Oncol. 2017;28(6): 1191–206. https://doi.org/10.1093/annonc/mdx034
21. Li R, Chen T-W, Wang L-Y, Zhou L, Li H, Chen X-L, et al. Quantitative measurement of contrast enhancement of esophageal squamous cell carcinoma on clinical MDCT. World J Radiol. 2012;4(4):179–85. https://doi.org/10.4329/wjr.v4.i4.179
22. Wu X, Han R, Zhong Y, Weng N, Zhang A. Post treatment NLR is a predictor of response to immune checkpoint inhibitor therapy in patients with esophageal squamous cell carcinoma. Cancer Cell Int. 2021;21(1):1–10. https://doi.org/10.1186/s12935-021-02072-x
23. Jin W, Luo Q. When artificial intelligence meets PD-1/PD-L1 inhibitors: population screening, response prediction and efficacy evaluation. Comput Biol Med. 2022;145:105499. https://doi.org/10.1016/j.compbiomed.2022.105499
24. Huang W, Jiang Y, Xiong W, Sun Z, Chen C, Yuan Q, et al. Noninvasive imaging of the tumor immune microenvironment correlates with response to immunotherapy in gastric cancer. Nat Commun. 2022; 13(1):5095. https://doi.org/10.1038/s41467-022-32816-w
25. Zheng Y-m, Yuan M-g, Zhou R-q, Hou F, Zhan J-F, Liu N-D, et al. A computed tomography–based radiomics signature for predicting expression of programmed death ligand 1 in head and neck squamous cell carcinoma. Eur Radiol. 2022;32(8):5362–70. https://doi.org/10.1007/s00330-022-08651-4
26. Cui H, Zeng L, Li R, Li Q, Hong C, Zhu H, et al. Radiomics signature based on CECT for non-invasive prediction of response to anti-PD-1 therapy in patients with hepatocellular carcinoma. Clin Radiol. 2023; 78(2):e37–44. https://doi.org/10.1016/j.ejrad.2017.11.007
27. Van Griethuysen JJ, Fedorov A, Parmar C, Hosny A, Aucoin N, Narayan V, et al. Computational radiomics system to decode the radiographic phenotype. Cancer Res. 2017;77(21):e104–7. https://doi.org/10.1158/0008-5472.CAN-17-0339
28. Lemaître G, Nogueira F, Aridas CK. Imbalanced-learn: a python toolbox to tackle the curse of imbalanced datasets in machine learning. The Journal of Machine Learning Research. 2017;18(1):559–63. https://doi.org/10.48550/arXiv.1609.06570